Check for updates

# Interrogating the missing links in tandem $CO_2$ hydrogenation: role of intermediate transport, active site proximity, and ion exchange in zeolites

Fatima Mahnaz, Andrew Iovine and Manish Shetty [ID] *

The tandem hydrogenation of $CO_2$ to fuels and chemicals using bifunctional oxide/zeolite catalysts offers a promising strategy for reducing anthropogenic $CO_2$ emissions while generating sustainable alternatives to fossil fuels. Despite significant advancements in this field, fundamental gaps remain in understanding the inflence of active site-proximity, intermediate transport rates, and the metal oxide migration and their ion-exchange with zeolitic Brønsted acid sites (BAS) on the reaction rates and hydrocarbon (HC) product selectivities. Challenges also include high CO selectivity and understanding the complexities of hydrocarbon pool (HCP) propagation in zeolite pore channels. This perspective integrates insights from analogous bifunctional catalytic systems, such as alkane hydrocracking and isomerization, to refine our understanding of site-proximity and transport artifacts on reaction rates and product selectivities. We examine diffusion-reaction formalisms for elucidating site-proximity effects on rates and HC selectivity, discuss methods to suppress CO selectivity using surface organometallic chemistry (SOMC) approaches, and explore strategies for suppressing ion-exchange and tuning HCP dynamics. By addressing these challenges, we outline a conceptual roadmap for advancing tandem $CO_2$ hydrogenation chemistry, providing potential strategies to enhance catalytic efficiency of bifunctional oxide/zeolite systems.

## Introduction

Catalytic tandem reactions have emerged as a powerful tool in chemical synthesis, enabling multi-step transformations within a single system while enhancing energy efficiency[1] and breaking

*Artie McFerrin Department of Chemical Engineering, Texas A&M University College Station, TX 77843, USA. E-mail: manish.shetty@tamu.edu*

or circumventing selectivity-activity tradeoffs.[2] This selectivity-activity limitation is described by Sabatier's principle, which states that an ideal catalyst should bind reactants neither too strongly nor too weakly to achieve optimal performance.[2–5] However, this balance is often difficult to maintain in single-site catalysts, as strong binding enhances activation but risks poisoning, while weak binding limits reactivity.[5,6] Tandem catalysis mitigates this limitation by utilizing multiple catalytic

*Fatima Mahnaz is a PhD candidate in chemical engineering at Texas A & M University, specializing in heterogeneous catalysis. She earned her BSc in Chemical Engineering from the Bangladesh University of Engineering and Technology in 2018. Her research focuses on developing bifunctional catalysts for $CO_2$ hydrogenation to sustainable fuels and chemicals, with an emphasis on tandem catalysis and site proximity effects. Passionate about sustainable energy, she aspires to contribute to advancements in carbon-neutral fuel technologies.*

**Fatima Mahnaz**

*Andrew Iovine is a senior undergraduate student pursuing a BS in chemical engineering at Texas A & M University. He joined Prof. Manish Shetty's lab in Spring 2025 and is interested in gaining a better understanding of heterogeneous catalysis. After graduation, he plans to pursue a PhD to further study topics in catalysis and reaction engineering field.*

**Andrew Iovine**

sites with distinct functions, enabling selective activation and intermediate transformation at different stages of the reaction.[2] Hence, researchers have increasingly applied tandem catalysis principles to heterogeneous catalytic processes,[7–15] particularly in the field of $CO_2$ hydrogenation.[16–30]

Tandem reactions typically involve bifunctional catalytic cascades, with an intermediate forming over one active site and its subsequent conversion over a different active site. Kumar *et al.* demonstrated that in such cascading systems, the two distinct functionalities (*e.g.*, metal and acid sites, metal and metal-support interface sites, *etc.*) exhibit different Brønsted–Evans–Polanyi (BEP) scaling relationships for the same intermediates along the reaction pathway and can potentially enhance reaction rates by leveraging separate mechanistic contributions, thereby breaking the selectivity-activity limits.[6] While the idea of breaking selectivity-activity limits and converting $CO_2$ to carbon-neutral fuels and chemicals seem appealing, designing efficient catalysts that maximize the utilization of all active sites and enhance selectivity toward desired product is challenging.

During tandem reactions, including $CO_2$ hydrogenation, over bifunctional catalytic systems, the two catalytic functions are linked *via* the shuttling of reaction intermediates, thus requiring "site-proximity", which ensures that active sites are spatially arranged to facilitate sequential transformations by minimizing the diffusion distance of intermediates. As such, the transport of intermediates between active sites (*e.g.*, redox and Brønsted acid sites) can influence overall rates and selectivities,[31] complicating the interpretation of intrinsic kinetics and reaction mechanism.

In tandem $CO_2$ hydrogenation to hydrocarbons (HCs) in the methanol ($CH_3OH$)-mediated route, $CH_3OH$ initially forms over redox sites (or oxygen vacancies) or alloys on metal oxides and then subsequently undergoes dehydration and C–C coupling over Brønsted acid sites (BAS) of zeolites to form HCs.[32] This sequential reaction steps make site-proximity particularly crucial for this chemistry as the intermediate $CH_3OH$ must efficiently transport from redox sites to BAS for the methanol-to-hydrocarbon (MTH) conversion. Recent studies, including our



**Manish Shetty**

*Prof. Manish Shetty is an Assistant Professor in the Artie McFerrin Department of Chemical Engineering at Texas A & M University since Fall 2021. He earned his B.Tech. and M.Tech. in Chemical Engineering from the Indian Institute of Technology Bombay in 2011 and his PhD from the Massachusetts Institute of Technology. He currently leads a research group in heterogeneous catalysis and sustainability, with an emphasis on industrial decarbonization, plastics valorization, hydrogen storage, and improving the efficiency of catalyst materials.*
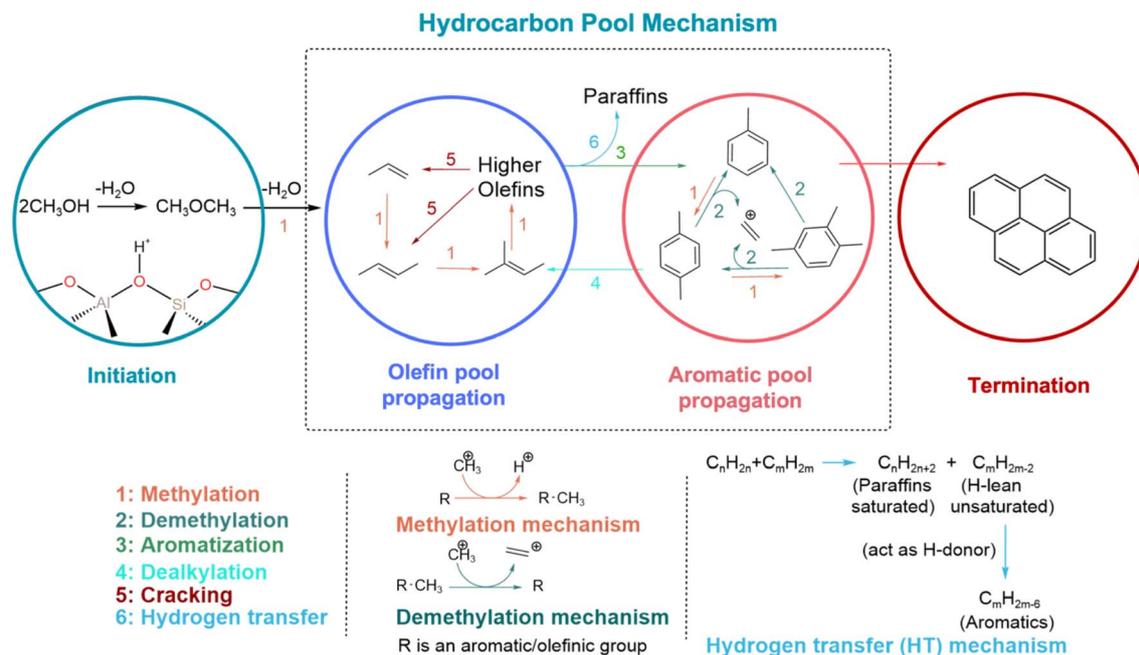
own, have demonstrated that the efficacy of bifunctional oxide/zeolite systems is largely dictated by the efficiency of $CH_3OH$ transport and its consumption over BAS.[16,33,34] As such, the catalytic efficiency can be enhanced by improving the site proximity between redox sites and BAS.[31] However, at the closest proximity (*i.e.*, nanoscale distance), two key problems exist; (1) the catalytic performance could be hindered by the migration of metal oxides inside zeolite framework and their cation exchange with BAS,[17,26,27,35–38] and (2) the improvement in hydrocarbon (HC) yields and formation rates do not necessarily scale with the rate of $CH_3OH$ transport.[31] As such, the molecular underpinnings of proximity-effects are convoluted and yet not understood for this conversion.

Additional key challenge associated with the $CH_3OH$ mediated route is the high CO selectivity caused by the endothermic side reaction of reverse-water–gas-shift (RWGS), which reduces hydrocarbon yield.[32] While CO selectivity can be reduced by conducting reactions at low temperatures, the low reaction rates make it difficult to achieve appreciable single-pass $CO_2$ conversions. In addition to that MTH is favored at higher reaction temperatures.[32] Therefore, increasing HC yield while keeping CO selectivity low becomes a formidable challenge in this route and requires better $CH_3OH$ synthesis catalysts.

It is to be noted that while HC yields can potentially be enhanced by increasing $CH_3OH$ yield, achieving precise control over HC selectivity requires a fundamental understanding of how hydrocarbons form within zeolite pore channels.[39] The reaction proceeds *via* a chain carrier mechanism consisting of three distinct phases: initiation, propagation, and termination (Fig. 1).[39,40] During the initiation phase, unsaturated hydrocarbons form within the micropores of zeolite. These intermediates then participate in the propagation phase, following the well-established "dual cycle" or hydrocarbon pool (HCP) mechanism, which consists of two interconnected pathways: (1) the olefin cycle, where olefins undergo sequential methylation and cracking, and (2) the aromatic cycle, where aromatic species undergo methylation and demethylation. The interplay between these two cycles occurs through the aromatization of olefins and the dealkylation of aromatics to olefins, ultimately governing hydrocarbon selectivity.[39] Although extensive research has focused on modulating the HCP mechanism in MTH conversion through changing reaction conditions, such as co-feeding $H_2$ or CO, or changing zeolite composition, such as adjusting the Si/Al ratio of the zeolite or tuning acid site strength,[41] the reaction conditions and catalytic system employed for tandem $CO_2$ hydrogenation is different. A deeper understanding of the factors influencing the HCP mechanism in $CO_2$ hydrogenation is therefore essential for achieving selective conversion to targeted hydrocarbon products.

Overall, despite advances in bifunctional catalyst design, the efficiency of $CO_2$ hydrogenation to selective HC remains constrained by critical knowledge gaps. Key unresolved questions include: (i) What does the "site-proximity" effect entail in tandem $CO_2$ hydrogenation? (ii) What is the role of site-proximity in the transport of reaction intermediates? (iii) Can advection-diffusion-reaction formalisms be leveraged to interpret the proximity effect and its impact on reaction rates and

**Fig. 1** Hydrocarbon pool (HCP) mechanism of methanol-to-hydrocarbon (MTH) conversion inside zeolite pore channels including initiation, propagation, and termination phases. The propagation encompasses multiple steps, including olefin methylation, cracking, hydrogen transfer, aromatization, aromatic methylation, and aromatic dealkylation. Adapted with permission from Mahnaz, F. & Shetty, M. *et al.*[38] Copyright *J. Catal.* 2024.

selectivity? (iv) How do metal oxide migration and cation exchange occur at intimate proximities, and what are their effects on reactivity? (v) What strategies can reduce CO selectivity to enhance hydrocarbon yields? and (vi) How can HC selectivity be controlled through modulating HCP?

To address these challenges, this perspective explores insights into proximity effects derived from analogous bifunctional catalytic systems, such as alkane hydrocracking and isomerization chemistry, which share mechanistic parallels with tandem $CO_2$ hydrogenation. We examine seminal work by Weisz[42–44] and Iglesia[45,46] on *n*-heptane isomerization, applying diffusion-reaction mathematical formalisms to different proximity length scales to elucidate intermediate transport effects. Additionally, we analyze how catalyst modifications at intimate proximities-*via* metal oxide migration and cation exchange at redox and acid sites can influence reaction pathways and propose strategies to mitigate these effects. Furthermore, we discuss approaches to overcoming the intrinsic challenge of CO selectivity by employing surface organometallic chemistry (SOMC) to enhance $CH_3OH$ selectivity and yield.[47,48] Finally, we explore methods to modulate HCP to control HC selectivity. By integrating these perspectives, we aim to provide a roadmap for advancing $CO_2$ hydrogenation through fundamental insights into site-proximity effects, catalyst design, and reaction engineering strategies.

### Proximity-effects and role of intermediate transport

Research into the impact of site proximity in bifunctional systems dates back to the 1950s for enhancing the efficiency of alkane isomerization,[43,44] which involve similar bifunctional catalytic cascades akin to $CO_2$ hydrogenation with alkanes first

forming alkenes on a metal function, alkenes undergoing skeletal isomerization or C–C bond cleavage on an acid function, and their products hydrogenating at the metal function to form their saturated analogs. It was observed that enhancing the proximity between active sites (metal sites on $Pt/SiO_2$ for hydrogenation and dehydrogenation activity and acid-sites on mesoporous $SiO_2–Al_2O_3$ for isomerization) *via* modulating their particle size, increased the local concentration of intermediates, driving higher diffusive flux and enabling more efficient conversion (Fig. 2).[42] Therefore, the proximity-dependent reactivity was attributed to the internal mass transport limitation of the reaction intermediate. Weisz quantified this proximity requirement as a function of intermediate vapor pressure by applying the condition where reaction rate on the surface would be equal to the net diffusive flux (eqn (1)),[44]

$$\frac{dN_s}{dt} = D_{eff}|grad C|_{R=R_0} \tag{1}$$

where $\frac{dN_s}{dt}$ is the surface reaction rate, $D_{eff}$ is the effective internal diffusion, $C$ is the reactant/intermediate concentration and $R_0$ is the catalyst particle size. For the case of negligible inhibition from rate by diffusion, the following condition was assumed,

$$|grad C|_{R=R_0} \ll \frac{C_0}{R_0} \tag{2}$$

where $C_0$ is the external concentration of reactant/intermediate. By combining these expressions, Weisz derived a criterion for determining the maximum catalyst particle size ($R_c$) to avoid diffusion limitations,
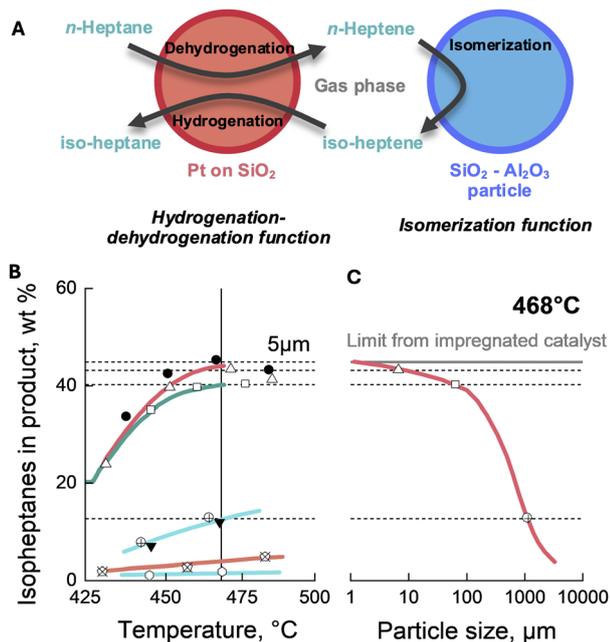
**Fig. 2** (A) Schematic of *n*-heptane isomerization over Pt/SiO$_2$ and SiO$_2$–Al$_2$O$_3$ catalyst. (B) Influence of temperature and particle size on the selectivity of iso-heptane in the product. (C) Influence of particle size on iso-heptene selectivity. Adapted with permission from Weisz.[42] Copyright *Adv. Catal.* 1962.

$$\frac{\mathrm{d}N_s}{\mathrm{d}t} \frac{1}{C_0} \frac{R_c^2}{D_{\text{eff}}} \ll 1 \quad (3)$$

Applying this criterion, Weisz demonstrated that for an intermediate species with a partial pressure of $10^{-3}$ atm (as might be observed in olefin production during hydrocarbon reactions), the maximum catalyst particle size should be around 50 μm to avoid diffusion constraints in mesoporous catalysts (Fig. 3). Interestingly, even when an intermediate exists at a partial pressure of $10^{-10}$ atm, a stepwise reaction could still proceed without diffusion limitation, provided that the catalytic
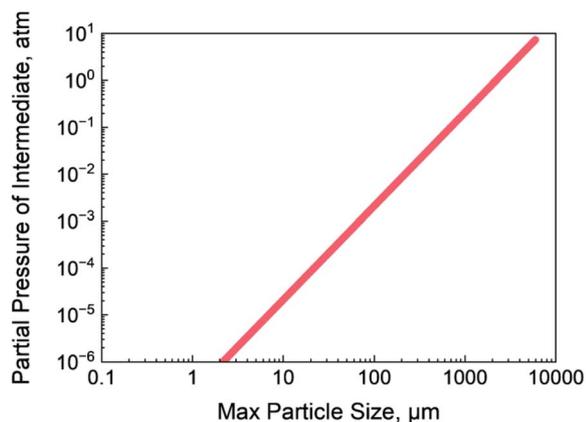


**Fig. 3** Proximity requirement, in terms of component particle size, for typical conditions of reaction rate ($10^{-6}$ moles s$^{-1}$ cm$^{-3}$), as a function of equilibrium vapor pressure of intermediate. Adapted with permission from Weisz.[42] Copyright *Adv. Catal.* 1962.

sites are within $\sim$100 Å (10 nm) of each other.[44] This finding underscores the critical role of site proximity in bifunctional catalysis, where intermediate transport between distinct active sites governs overall catalytic performance.

Akin to hydrocarbon hydroisomerization and hydrocracking reactions, for tandem CO$_2$ hydrogenation, there is a consensus that the HC selectivity could be enhanced by improving CH$_3$OH transport from active sites on metal oxides (*e.g.*, oxygen vacancy sites) to BAS by improving their proximity.[18,49,50] However, the improvement in hydrocarbon yields and formation rates do not necessarily scale with the rate of intermediate CH$_3$OH transport (estimated from the ratio of linear velocity and distance between the active sites).[31] It is our conjecture that a possible reason could be the diffusional restriction of HC inside microporous zeolites as the acid sites reside within voids of molecular dimensions, restricting their diffusional egress. Therefore, the physical characteristics of the diffusive medium, such as channel size, connectivity, crystal size, and the number of acid sites can become consequential for measured reaction rates.[41] We emphasize that using microporous zeolites makes it difficult to apply Weisz's proximity criterion to find a critical length scale with negligible diffusion limitation, as the constituent reactions in MTH involving bulkier hydrocarbons would be inherently mass transport limited. In such systems, where transport artifacts influence selectivity in complex reaction networks, the Thiele modulus ($\phi_A$) emerges as a fundamental non-dimensional parameter for analysis.[51,52]

$$\phi_A^2 = \frac{k_n C_A^{n-1} \rho^*}{\dfrac{D_A}{R^2}} \quad (4)$$

where $D_A$ is the effective diffusivity of molecule A, $k_n$ is the *n*-order rate constant normalized by number of active sites, and $\rho^*$ is volumetric active site density, $R$ is characteristic length of the catalyst particle/crystallite.

Thiele modulus naturally arises from a mole balance on the reactive domain of a catalyst and is defined as the ratio of the intrinsic reaction rate (in absence of mass transport limitation) to the diffusion rate when the driving force is at its maximum (eqn (4)). A low $\phi_A$ value (<1) indicates minimal mass transport limitations, allowing measured reaction rates to reflect intrinsic kinetics.[51,52] As reactant concentration gradients become more pronounced, $\phi_A$ increases and leads to diffusion constraints that suppress observed reaction rates ($r_{A,\text{meas}}$) relative to their kinetic counterparts ($r_{A,\text{kinetic}}$). This discrepancy can be quantitatively estimated through the effectiveness factor ($\eta_A$) (eqn (5)),[51,52] which measures the fraction of the intrinsic reaction rate achieved under diffusion-limited conditions.

$$\eta_A = \frac{r_{A,\text{meas}}}{r_{A,\text{kinetic}}} = \left[\frac{3}{\phi_A^2}(\phi_A \coth(\phi_A) - 1)\right] \quad (5)$$

For spherical catalyst particles, $\eta_A$ remains close to unity at low $\phi_A$ values, but declines as diffusional limitations increase.[51,52] This framework remains applicable across various catalyst geometries when generalized Thiele modulus and effectiveness factor expressions are employed.

The application of these principles to tandem or cascading catalytic systems, however, presents unique challenges. For

example, in such systems, if secondary reaction rates are faster than primary reaction rates and/or if the molecular diffusivities of primary products are low (*i.e.*, $\phi_A \gg 1$), diffusion limitations can obscure product identity.[46] For example, secondary reactions may take place before primary products can be detected in the bulk phase, complicating efforts to elucidate reaction networks and mechanisms.[53] Such occurrences necessitate careful diagnostic strategies to ensure accurate interpretation of catalytic performance. A classic example of this phenomenon is *n*-heptane isomerization over Pt/zeolite catalysts, where reactivity is influenced by the proximity of metal and acid sites.[45] The reaction sequence involves the formation of linear heptenes ($nH^=$) as a mixture of equilibrated regioisomers from *n*-heptane dehydrogenation on Pt sites. These $nH^=$ species subsequently undergo isomerization at acid sites to form 2-methylhexenes ($2MH^=$) and 3-methylhexenes ($3MH^=$), which can further isomerize into dimethylpentenes ($DMP^=$) (Fig. 4A). The $DMP^=$ isomers act as the precursors to β-scission products.[45] Iglesia and co-workers demonstrated that the selectivity toward β-scission products increases with increasing distance between metal and acid sites, highlighting the role of site-proximity on product selectivity.[45] Specifically, by dispersing Pt nanoparticles within zeolite crystals thus by increasing the intracrystalline Pt–H$^+$ distance (*via* decreasing Pt loading), they observed higher *n*-heptane conversion turnover rates (per H$^+$ site) and shifts in β-scission selectivity. To assess these transport effects on rates and selectivities, Iglesia and coworkers applied mathematical diffusion–reaction formalisms that account for intracrystalline gradients in reactant and product concentrations and for the local equilibration of alkene interconversion steps.[45,46] These descriptions were then embedded within a plug-flow convection-reaction formalisms to describe the distribution of products formed as concentration gradients developed within

crystallites and along the packed-bed reactor. This rigorous diffusion-convection-reaction analysis (Fig. 4B) linked the product selectivities to Thiele moduli, ultimately revealing that intrinsic selectivities were largely governed by diffusion-enhanced secondary reactions (Fig. 4C). These insights underscore the critical interplay between transport limitations and reaction kinetics in tandem/cascading systems. We emphasize that such analytical frameworks are equally critical for deciphering transport artifacts and the mechanistic intricacies involved in tandem $CO_2$ hydrogenation.

We note that, while evaluating the applicability of the Thiele modulus ($\phi_A$) to tandem $CO_2$ hydrogenation system, one may question its relevance given the relatively small size of key intermediates, $CH_3OH$, unlike bulky intermediates encountered in alkane isomerization (*e.g.*, *n*-heptene). Notably, the first step of $CH_3OH$ synthesis over metal oxide catalyst can be operated in kinetic regime without mass transport limitation.[54] Additionally, for the initiation step of MTH conversion, intermediate $CH_3OH$ have smaller kinetic diameter (3.6 Å)[55] than typically used zeolite pore size (3.8 Å for CHA, 3.8 Å for AFX, 8.35, 4.8 Å for LEV, 5.6 Å for MFI),[56] therefore, $CH_3OH$ transport in zeolite pores should not be diffusion limited (assuming negligible external mass transport effects). However, the propagation and termination sequences during MTH are mediated by active chain carriers (*e.g.*, dienes, branched olefins, aromatics *etc.*), which are transport-limited to varying extents depending on zeolite morphology, pore structure, and crystal size.[57,58] The presence of these species and their mass transport limitations impose spatial gradients during MTH on both bed and zeolite crystallite scales, complicating the interpretation of HC selectivity solely based on intrinsic kinetics.[57] In such scenarios, the observed volumetric formation rate for bulkier HC ($C_mH_n$), $r_{obs,\,C_mH_n}$, includes contributions from the intrinsic
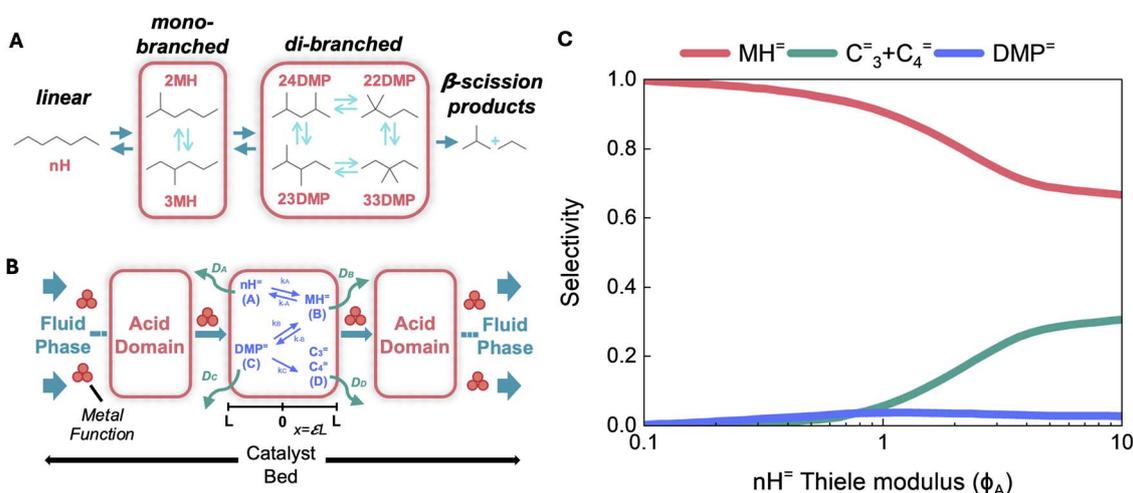


Fig. 4 (A) Isomerization and β-scission reaction network for C$_7$ alkenes on bifunctional physical mixtures of Brønsted acid catalyst and Pt/SiO$_2$. Dashed boxes around isomers with the same degree of branching indicate facile interconversion and isomers treated as a kinetic lump. (B) Schematic depiction of the coupled diffusion–convection–reaction system for bifunctional isomerization and -scission cascades. Acid domains are represented by the inset solid rectangles, the catalyst bed is denoted by the surrounding dashed rectangle. Metal functions and acid sites (H$^+$) are also displayed. (C) Selectivities to methyl hexenes (MH$^=$), dimethyl pentenes (DMP$^=$) and -scission products (C$_3^=$ + C$_4^=$) as a function of Thiele modulus, observed by modulating intracrystalline Pt–H$^+$ site distance by confining Pt in MFI. Adapted with permission from Hu, W. & Iglesia, E. *et al.*[45] Copyright *J. Catal.* 2023.

volumetric rates ($r_{int,p}$) for a reaction $p$ (*i.e.*, aromatic dealkylation, olefin methylation *etc.*) in the absence of mass transport limitations and an overall effectiveness factor ($\eta_p$) that quantitatively assesses diffusional constraints.[57]

$$r_{\text{obs, }C_mH_n} = \sum_p \nu, \ C_mH_n \ r_{\text{int, }p} \ \eta_p \qquad (6)$$

where, $\nu, _{C_mH_n}$ represents the stoichiometric coefficient associated with $C_mH_n$ in reaction $p$. The overall effectiveness factor ($\eta_p$) depends on Thiele modulus ($\phi_A$), which makes it relevant for tandem $CO_2$ hydrogenation. In this regard, to assess the diffusional constraints on the complex reaction network of MTH, Bhan and coworkers employed a combined parameter of H$^+$ density ($\rho_H^+$) multiplied to a functional assessment of crystallite size $\frac{\rho_{H^+}R^2}{D}$, where $R$ is the zeolite crystallite size and $D$ is the effective diffusivity of component $C_nH_m$.[59] During MTH on MFI, it was observed that increasing $\frac{\rho_{H^+}R^2}{D}$ (whether by changing zeolite crystal size or acid site density), increased ethylene ($C_2^=$) selectivity while other light olefin selectivities were invariant.[57] The increase in $C_2^=$ selectivity and invariance in light olefins selectivity resulted in an increase in ethylene-to-2-methyl-butane ($C_2^=$/2MB) ratio (indictive of the relative propagation of olefin cycle relative to aromatic cycle in HCP), as shown in Fig. 5A, suggesting an enhanced propagation of the aromatic cycle. From a mathematical perspective, this phenomenon was rationalized as a consequence of aromatics-based reactions (*e.g.*, aromatic dealkylation to ethylene formation) experiencing more severe transport limitations (*i.e.*, larger $\phi_A$) relative to the other reactions during MTH (*e.g.*, olefins methylation in olefin cycle) such that the rates and effectiveness factor prescribing aromatics cycle propagation depend more sensitively on diffusional constraints, described by,[57]

$$\frac{\partial(\text{selectivity of } C_2H_4)}{\partial \frac{\rho_{H^+}R^2}{D_{C_2H_4}}} \gg \frac{\partial(\text{selectivity of } C_mH_{2m, \ m \neq 2})}{\partial \frac{\rho_{H^+}R^2}{D_{C_mH_{2m}}}} \qquad (7)$$

For small cage zeolite with CHA framework, the influence of diffusional constraints was reflected on catalyst lifetime, assessed in terms of cumulative turnover number (TON), where the total turnovers decreased with increasing diffusional constraints regulated by $\frac{\rho_{H^+}R^2}{D}$ see (Fig. 5B).[41,58] Additionally, reaction-transport analysis of the MTO reaction network over SAPO-34 revealed that the effect of diffusional constraints on total turnovers was caused by dehydrocyclization reactions, which experience stronger diffusional constraints than olefins methylation, methanol transfer hydrogenation, and aromatics dealkylation.[58]

We note that the diffusional influence on HC product selectivity can further be probed by employing zeolites with varying undulation factor ($\Omega$), which represent the ratio of the maximum diameter HC that can diffuse from zeolite pore to that which can be occluded. Such techniques were utilized to probe diffusional effect on alkene oligomerization and $\beta$-scission.[53] Iglesia and coworkers revealed that both 1-D 10 membered-ring (MR) TON and mesoporous Al-MCM-41 mitigated $\beta$-scission reactions having less diffusional effect ($\Omega \sim 1$) while zeolites with smaller undulation factor, like MFI and FAU, had broad product distributions, including significant amounts of $\beta$-scission products due to diffusion limitation (Fig. 6).[60] As such, using zeolites with different undulation factor during $CO_2$ hydrogenation can provide valuable mechanistic insights by distinguishing between primary, secondary and diffusion enhanced reaction pathways.

### Role of site-proximity on thermodynamics constraints

Thermodynamically, $CH_3OH$ synthesis from $CO_2$ hydrogenation is not equilibrium-limited at low temperatures (below ~250 °
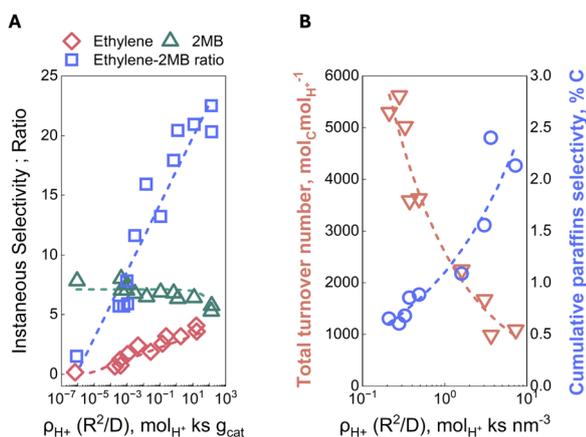


**Fig. 5** (A) Instantaneous ethylene and 2MB (2-methylbutane, 2-methyl-2-butene) selectivity, ethylene-to-2MB ratio *versus* $\frac{\rho_{H^+}R^2}{D}$ for DME conversion over HZSM-5 of varying crystallite size and Si/Al ratio at 623 K. (B) Total turnover number (left axis) and cumulative paraffins selectivity (right axis) for methanol conversion on HSAPO-34 at 673 K, 16 kPa methanol pressure. Adapted with permission from Bhan and coworkers.[59] Copyright *J. Catal.* 2023.
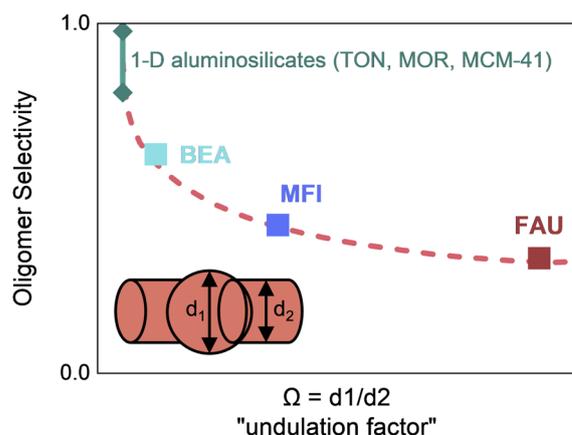


**Fig. 6** Selectivity to oligomers (*i.e.*, not $\beta$-scission products) as a function of the diffusion pathway in zeolites. The undulation factor is defined as the ratio of the largest cavity to pore-limiting diameters. Adapted with permission from Sarazen, M. L. *et al.*[60] Copyright *ACS Catal.* 2016.

C),[61] although the kinetics become slower resulting in a low single-pass $CO_2$ conversion. However, at higher reaction temperatures, the reaction becomes equilibrium-limited due to the negative entropy of the reaction ($\Delta G = \Delta H - T\Delta S$),[62–64] limiting $CH_3OH$ yield. Yet high reaction temperatures (350–400 °C) are needed for tandem $CO_2$ hydrogenation as MTH conversion is favorable >350 °C.[65,66] Remarkably, despite the unfavorable equilibrium shift for $CH_3OH$ synthesis at high temperatures, coupling with the MTH reaction drives the overall tandem reaction forward *per Le Chatelier's* principle, since $CH_3OH$ is simultaneously consumed as an intermediate and converted into thermodynamically more stable olefins and aromatics.[64] Jones and coworkers conducted thermodynamic analyses on $CH_3OH$ synthesis from $CO_2$ hydrogenation, as well as $CO_2$ conversion to olefins and aromatics.[64] Their analysis indicates that the overall Gibbs free energies for the formation of olefins and aromatics are lower (*i.e.*, more negative) than the $CH_3OH$ synthesis reaction alone (see Fig. 7),[64,67,68] making the tandem reaction more thermodynamically favorable.[64,69] This interplay highlights the relevance of site proximity in modulating thermodynamic constraints. We anticipate that when metal oxide and zeolite domains are at intimate proximity, the consumption of $CH_3OH$ over adjacent acid sites can lower its effective partial pressure and potentially shift the equilibrium of $CH_3OH$ synthesis forward, facilitating higher HC yield. Thus, site proximity can potentially manipulate thermodynamic constraints, favoring $CH_3OH$ formation under conditions otherwise deemed equilibrium limited.

### Improving hydrocarbon yield

The formation of CO *via* endothermic RWGS can limit $CH_3OH$ yield, as it is favorable under tandem $CO_2$ hydrogenation conditions.[70,71] Strategies such as utilizing low reaction temperatures or adding CO as a co-feed to shift RWGS reaction equilibrium have been employed to mitigate the negative
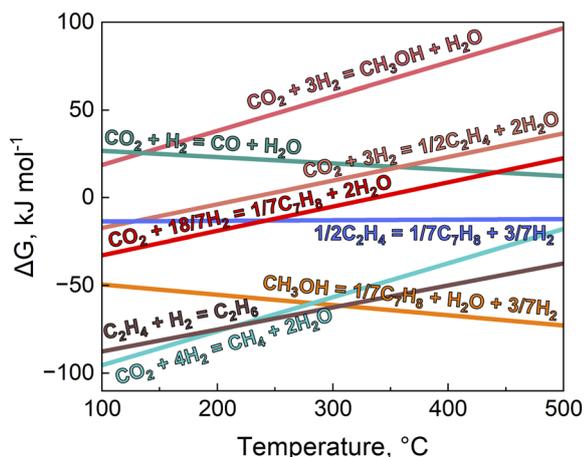
impact of CO formation on hydrocarbon yield.[26,27,72] However, an efficient way to reduce CO selectivity would be using a better $CH_3OH$ synthesis catalyst.

The hydrogenation of $CO_2$ to $CH_3OH$ is typically performed by catalysts consisting of copper and zinc ($Cu/ZnO/Al_2O_3$), and the reaction is commonly reported to proceed *via* formate and methoxy intermediates.[73–75] However, the formate species can also undergo decomposition to produce CO.[76,77] Based on these insights, we infer that the stabilization of methoxy species can potentially enhance $CH_3OH$ selectivity. A standout report in this context is the recent work by Copéret and coworkers where they incorporated Lewis acidic surface sites at the periphery of Cu to stabilize methoxy intermediates, thereby improving $CH_3OH$ selectivity by employing surface organometallic chemistry (SOMC) approach.[47] The authors synthesized a series of analogous catalysts containing Cu nanoparticles supported on $SiO_2$ decorated with metal centers of different Lewis acid strength ($Cu/M@SiO_2$, where M = Ti, Zr, Hf, Nb, Ta).[47] In this process, first, isolated *M* sites, free of organic ligands, were generated on $SiO_2$ by grafting a molecular precursor, *e.g.*, $M(OSi(O^tBu)_3)_m(O^iPr)_n$, followed by thermal treatment under vacuum to remove organic ligands (Fig. 8A). In the second step (Fig. 8B), Cu nanoparticles were generated on $M@SiO_2$ materials by grafting the copper precursor, $[Cu(O^tBu)]_4$ onto these $M@SiO_2$



Fig. 7 Gibbs free energy changes at different temperatures for $CH_3OH$ synthesis from $CO_2$ hydrogenation, $CO_2$ to lower olefins (ethylene), $CO_2$ to aromatics (toluene), and the reverse water-gas shift reaction. Simulated conditions for equilibrium $CO_2$ conversion: $H_2/CO_2 = 3$, total pressure 4 MPa. Adapted with permission from Jones and coworkers.[64] Copyright *J. $CO_2$. Util.* 2021.
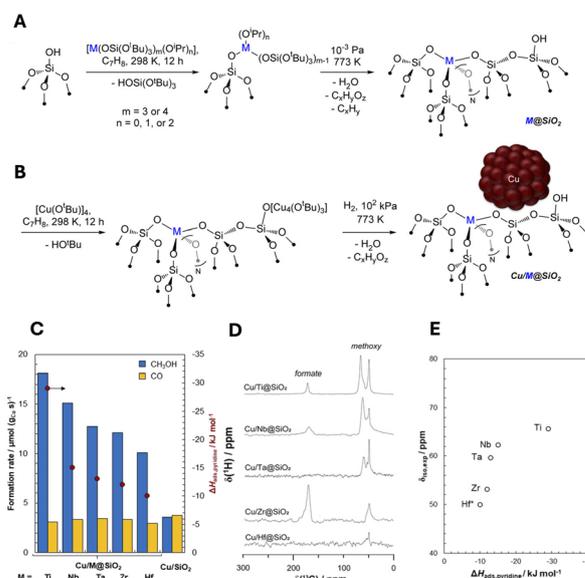


Fig. 8 Surface organometallic chemistry (SOMC) approach of catalyst synthesis. (A) Isolated M sites, free of organic ligands, were generated on $SiO_2$ by grafting a molecular precursor, *e.g.*, $M(OSi(O^tBu)_3)_m(O^iPr)_n$, followed by thermal treatment under vacuum to remove organic ligands. (B) Cu nanoparticles were generated on $M@SiO_2$ materials by grafting the copper precursor, $[Cu(O^tBu)]_4$ onto these $M@SiO_2$ materials, followed by a reductive thermal treatment. (C) Formation rate of $CH_3OH$ and CO over different $Cu/M@SiO_2$ catalyst. (D) $^{13}C$ solid-state NMR of formate and methoxy groups over different $Cu/M@SiO_2$ catalyst. (E) $^{13}C$ chemical shift of methoxy surface intermediates from solid-state NMR plotted against pyridine adsorption enthalpies to probe Lewis acid strength. Adapted with permission from Copéret and coworkers.[47] Copyright *Angew. Chem.* 2021.

materials, followed by a reductive thermal treatment. Interestingly, their investigation revealed that while CO formation rates (Fig. 8C) on these materials were nearly identical, $CH_3OH$ formation rates varied as a function of the identity of the M atom. The authors demonstrated that the promotion of $CH_3OH$ formation rates reflect the increasing acid strength of metal centers in $SiO_2$ support, probed by measuring $^{13}C$ chemical shift of methoxy surface intermediates from solid-state NMR (Fig. 8D) and pyridine adsorption enthalpies (Fig. 8E). These findings corroborated that the Lewis acid $M$ sites of these catalysts stabilize surface intermediates (formate and methoxy) at the periphery of Cu nanoparticles and influence $CH_3OH$ formation rates.[47]

In a similar SOMC approach, Copéret and coworkers showed that $CuGa_x$ alloy formed by grafting Cu on silica containing $Ga^{III}$ sites was highly active and selective for $CO_2$ hydrogenation to $CH_3OH$ (~90% selectivity at a conversion of ~3%).[48] Their investigation reported that under reaction conditions, the silica-supported $CuGa_x$ de-alloys yielding Cu nanoparticles and $Ga^{III}$ sites, which likely increased interfacial area between $Cu^0$ and $Ga^{III}O_x$ promoting $CH_3OH$ formation. Interestingly, only methoxy surface species were observed as intermediates probed *via* NMR and IR spectroscopy.[48] These findings highlight that stabilizing surface intermediates can improve $CH_3OH$ yields, offering a potential strategy to increase hydrocarbon yields during tandem $CO_2$ hydrogenation.

### Factors affecting hydrocarbon pool (HCP)

The formation of hydrocarbons inside zeolite pores proceeds *via* a dual cycle mechanism comprised of olefin and aromatic-based methylation/cracking events (Fig. 1).[39] The composition of HCP and the relative reactivity of various species in propagation and termination sequences across the catalyst bed govern the HC product selectivity. However, the kinetic and mechanistic elucidation of MTH remains challenging as the concentration and reactivity of olefinic and aromatic chain carriers vary as a function of catalyst properties and reaction conditions, leading to topology, morphology, composition, and time-dependent variations in MTH reaction rates and product selectivity.[59] For instance, small pore cage-window type zeolites favor a more aromatic HCP, or increasing BAS density shifts the HCP toward aromatics.[41] In the context of $CO_2$ hydrogenation, additional complexities arise, *e.g.*, co-presence of $H_2$ and CO which can further influence HCP. Therefore, a comprehensive understanding of the key factors governing HCP is essential to precisely tune hydrocarbon yield and selectivity in $CO_2$ hydrogenation.

Despite advances in bifunctional catalyst design, high CO selectivity remains an intrinsic challenge in $CO_2$ hydrogenation. While CO is often considered an undesired byproduct, recent insights from MTH chemistry suggest that it may play an active role in tuning HCP. Bhan and coworkers demonstrated that CO is mechanistically relevant in increasing ethylene-to-propylene (1.5–3×) and ethylene-to-methylbutenes (1.7×) ratio, both of which indicate a shift in the relative propagation of the aromatic to olefin cycle.[78] Additionally, CO can participate in

Koch carbonylation reactions with DME, promoting aromatic-cycle propagation and enabling ethylene formation *via* methyl acetate intermediates.[41] Despite these insights, the influence of CO in HCP and HC product selectivity in $CO_2$ hydrogenation remain largely unexplored, warranting the need for targeted investigations into how CO can be leveraged as a potential tuning parameter for HC selectivity.

Regarding the influence of $H_2$ on hydrocarbon selectivity, our recent study has shown that during $CO_2$ hydrogenation, the presence of $H_2$ promotes olefin cycle propagation over the aromatic cycle by facilitating secondary hydrogenation of olefins to paraffins.[38] This suppresses olefin aromatization and the formation of deactivation-inducing polycyclic aromatics, thereby mitigating the deactivation of acid function, which is an advantage compared to MTH conversion where zeolites deactivate *via* coking.[79] However, we anticipate that this may also present a stability-selectivity tradeoff, as the suppression of olefin aromatization will likely reduce aromatic selectivity during $CO_2$ hydrogenation to aromatics. Therefore, a detailed understanding of the role of $H_2$ on HCP is essential for optimizing targeted hydrocarbon selectivity.

The composition of zeolites also plays a critical role in shaping HCP and influencing HC selectivity. In this context, our recent study examined the impact BAS strength within the chabazite (CHA) framework on olefin selectivity during $CO_2$ hydrogenation by employing aluminosilicate SSZ-13 and silicoaluminophosphate SAPO-34, both possessing similar acid site densities.[38] When integrated as an interpellet admixture with $In_2O_3$, SSZ-13 predominantly facilitated secondary hydrogenation of olefins, yielding ~93% paraffins. In contrast, the $In_2O_3$/SAPO-34 admixture produced ~67% olefins, as the weaker acid strength of SAPO-34 resulted in a lower degree of secondary hydrogenation.[38] These findings underscore acid site strength as a crucial parameter for regulating HCP composition and hydrocarbon selectivity. We note that beyond acid strength, acid site density (represented by the Si/Al ratio), also influences HCP dynamics. In this regard, Chen *et al.* investigated SSZ-13 with varying Si/Al ratios integrated with $ZnZrO_x$ and demonstrated that SSZ-13 with only isolated acid sites (*i.e.*, high Si/Al ratio ~125) effectively mitigated the over-hydrogenation of light olefins to alkanes, thereby enhancing light olefin selectivity (~89%) compared to lower Si/Al ratio (~9, yielded ~93% paraffins) counterpart.[28] These findings highlight the tunability of zeolite acidity as a powerful tool for modulating HCP composition and optimizing hydrocarbon selectivity during $CO_2$ hydrogenation.

### Solid-state ion-exchange (SSIE) in zeolites

A fundamental challenge in designing efficient bifunctional oxide/zeolite catalysts lies in optimizing the proximity between redox and acid sites. While nanoscale proximity facilitates intermediate transport, it also introduces a caveat of metal oxide migration into zeolite pore channels, leading to solid-state ion exchange (SSIE) with BAS under the harsh reaction conditions (300–450 °C and 20–50 bar pressure).[17,35] We note that such SSIE could be avoided by i) conducting reaction at low

temperatures and/or ii) employing stable non-migrating metal oxides for $CH_3OH$ synthesis (*e.g.*, $ZrO_2$), however, both of these strategies would decrease HC yield as MTH is favorable at higher reaction temperatures and thermally stable metal oxides with fewer oxygen vacancy sites cause less $CH_3OH$ yield, respectively.[32,80–83] Therefore, elucidating the mechanistic pathways of SSIE and developing strategies to prevent it without compromising catalytic efficiency is a key to designing robust and selective oxide/zeolite catalysts for tandem $CO_2$ hydrogenation.

## Mechanistic insights on SSIE

A solid-state reaction $(M_n^+O_2^{n/2} + nH^+Z^- \rightarrow M_n^+Z_n^- + nH_2O\uparrow)$ between a zeolite and an oxide, which contains the desired in-going cation, necessitates their intimate contact, *e.g.*, typically achieved through milling or grinding.[84–86] This makes SSIE particularly relevant for tandem $CO_2$ hydrogenation, where milling or grinding are often employed to increase the proximity of redox sites and BAS for efficient intermediate transport.[22,23,87] Additionally, SSIE requires a reaction temperature of 400–625 K, which falls in the typical operating range for $CO_2$ hydrogenation.[35,88,89] As such, careful consideration is required to avoid SSIE and preserve the reactivity of the redox and acid sites. In principle, the transport of in-going cations can proceed through either vapor-phase or surface diffusion mechanisms.[90–93] While metals like zinc (Zn) and gallium (Ga) are likely exchanged *via* intracrystalline gas-phase transport, many metal oxides such as $(CuCl_2)$ exhibit low vapor pressures, even at elevated temperatures, making vapor-phase transport less feasible.[92] As a result, surface diffusion from the closely contacted oxide to the zeolite particles is considered to be the more dominant mechanism in SSIE.[91] However, in either case, the question then remains as to whether ions or molecules of the respective compound diffuse into the zeolite pores after separation or as intact species. Both possibilities are shown schematically in Fig. 9.

In this regard, previous studies suggested that for medium-pore zeolite ferrierite, H-FER, SSIE was not observed with $LaCl_3$ as $LaCl_3$ molecule was too bulky to be able to penetrate

the 8 MR pore openings of H-FER.[90–93] This indicates that the mechanism of molecular diffusion is more likely to hold. This assumption was further supported by experiments of SSIE of H-ZSM-5 with molecules containing bulky anions (*e.g.*, salts of heteropoly acids such as $Cs_3[PW_{12}O_{40}]$).[90–93] Compared to the exchange CsCl, SSIE with $Cs_3[PW_{12}O_{40}]$ occurred only to a minor extent, due to partial decomposition of the salt. These studies suggested that the molecules did not dissociate but rather migrated as an intact species for SSIE (top scheme of Fig. 6).

### Influence of SSIE on hydrocarbon pool (HCP) mechanisms

Given that SSIE occurs at intimate proximities between redox and acid sites, its catalytic influence on $CO_2$ hydrogenation must be carefully assessed, as it can obscure the intended proximity effects.[94,95] Prior studies have demonstrated that SSIE in zeolites can create new active sites, altering HCP mechanism and subsequently affecting HC yield and selectivity. For instance, exchanging the BAS of HZSM-5 with zinc or gallium cations enhanced olefin aromatization,[96] while the exchange of BAS in β-zeolite with iron, chromium, or manganese cations promoted oligomerization of lower olefins.[97] In the context of tandem $CO_2$ hydrogenation, our recent findings reveal that the nature of the exchanged cation dictates distinct influences to HCP.[82] Specifically, SSIE between BAS of SAPO-34 and $In^{\delta+}$ species shut down HCP propagation inside the channels of SAPO-34 by inhibiting the acidity of SAPO-34, while SSIE with $Zn^{\delta+}$ species enhanced hydrogen transfer and secondary hydrogenation likely by creating Lewis acidic sites.[82] These SSIE-induced modifications were systematically probed using two key performance metrics: $C_3$ (propane + propylene)/$C_2$ (ethane + ethylene) ratio and paraffin-to-olefin (P/O) ratio during $CO_2$ hydrogenation, which convey the relative propagation of the olefin cycle to the aromatic cycle, and the degree of saturation of olefins in HCP, respectively.[59] Using these performance metrics, coupled with the occluded HC analysis and $^{13}C$ solid-state nuclear magnetic resonance (ssNMR) spectroscopy revealed that ion exchange of BAS with $In^{\delta+}$ and $Zn^{\delta+}$ species influenced the olefin and aromatic pool propagation, consequently altering HC selectivity and yield. These findings underscore the necessity of preventing SSIE of acid sites to mitigate unintended catalytic modifications during $CO_2$ hydrogenation.

### Mitigating SSIE

Mitigating SSIE in oxide/zeolite systems requires a fundamental understanding of the key factors driving ion exchange, including contact-induced metal oxide migration, volatility-driven gas-phase transport, reduction-assisted SSIE, and moisture-assisted SSIE (Fig. 10).[84,92] Identifying the predominant factor is crucial for developing effective mitigation strategies. For instance, volatility-driven SSIE can be assessed by tracking the amount of volatile component in metal oxide, such as Zn in $ZnZrO_x$, after thermal treatment at different temperatures using energy-dispersive X-ray spectroscopy (EDX).[98] By correlating the Zn loss with *in situ* acid site characterization, such as transmission FTIR using pyridine as a probe, the extent of BAS exchange with Zn at different temperatures due to
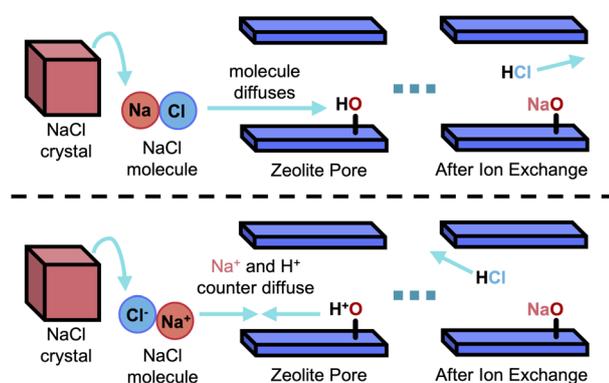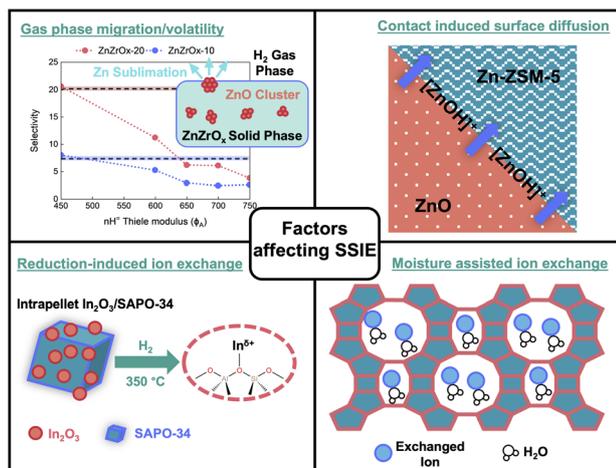


**Fig. 9** Schematic of two possible mechanism of SSIE. Top scheme: NaCl molecule diffuse, bottom scheme: $Na^+$ and $Cl^-$ counter diffuse. Adapted with permission from Karge, H. G.[92] Copyright *Catal. Today* 2008.

**Fig. 10** Factors affecting SSIE including volatility-driven gasphase transport (adapted with permission from Redekop, E. A. *et al.*[98]), contact-induced migration (adapted with permission from Wang, Y. *et al.*[17] Copyright *Angew. Chem. Int. Ed. Engl.* 2021), reduction-assisted SSIE (adapted with permission from Mahnaz, F. *et al.*[82] Copyright *Chem. Catal.* 2024), and moisture-assisted SSIE.

volatility can be estimated.[99] We expect such analyses would help determining the optimal operating temperatures to minimize acid site loss.

Contact-induced SSIE can be assessed by varying the proximity between redox and acid sites, as evidenced by our recent study showing that despite ZnO being highly volatile, SSIE was less prominent when $ZnZrO_X$ was integrated at a microscale distance from BAS of SAPO-34 compared to a nanoscale distance, indicating contact-induced diffusion as the dominant mechanism.[82] In such cases, core–shell confinement strategies to create diffusive barriers (*e.g.*, silicalite-1, silica, or alumina) between redox and acid sites can potentially mitigate SSIE.[100]

Additionally, SSIE can be enhanced under reductive conditions, as observed in our studies where SSIE between BAS of SAPO-34 and $In^{\delta+}$ was more drastic in the presence of $H_2$, as compared to inert environment.[82] Moisture may also facilitate SSIE by stabilizing cations, similar to conventional ion exchange process.[92,101,102] In certain cases, moisture aids SSIE by disaggregating oxide species or inhibiting their polymerization. For instance, moisture facilitated the SSIE of acid sites in Y-zeolites with $MoO_3$,[84] whereas in dry conditions, the $MoO_3$ species were too bulky to effectively undergo SSIE.[103] In such cases, employing hydrophobic coatings on metal oxides or zeolites could be a potential strategy to limit the interactions between BAS and oxide species, limiting excessive SSIE.[100] By systematically probing these factors, a more robust framework for suppressing SSIE could be developed, preserving the reactivity of oxide/zeolite bifunctional catalysts.

### Future outlook

This perspective highlights the critical challenges in $CO_2$ hydrogenation *via* the $CH_3OH$-mediated route and potential strategies to circumvent them, focusing on bridging the existing research gaps in the field. A key challenge in using bifunctional oxide/zeolite systems is that the proximity of active sites on metal oxides and BAS plays a crucial role in determining intermediate concentration gradients in acid site domain, therefore mass transport artifacts influence reaction rates and selectivities. Therefore, for elucidating "site-proximity" effect in $CO_2$ hydrogenation, we emphasize on developing diffusion-convection-reaction formulation along with experimentally probing the diffusion artifacts on the selectivity of bulkier hydrocarbons inside zeolite pores. We further propose that, since MTH conversion is inherently mass transport limited, these limitations should be leveraged to control product selectivities by tuning zeolite properties and pore architecture to control diffusion pathways. Probing diffusional effects by using zeolites with different crystallite size and undulation factors may help identifying primary and secondary products and optimizing reactivity and selectivity. When combined with reaction-transport models, these approaches could provide a comprehensive strategy for understanding diffusional influence on observed rates and HC selectivity.

Beyond the effects of active-site proximity and intermediate transport, we emphasize on understanding the implications of SSIE of acid sites on rates and HC selectivities and strategies to mitigate it. While conventional acid site characterization methods can detect ion exchange, we propose utilizing useful metrics, such as the propylene-to-ethylene, ethylene-to-2 methyl-butane, paraffin-to-olefin ratios *etc.*, to get better insights into how SSIE influences HCP mechanisms, altering HC selectivities.

A significant challenge in $CO_2$ hydrogenation is the high CO selectivity caused by the RWGS as a side reaction. To tackle this challenge, we emphasize increasing $CH_3OH$ yields. An example is innovative synthesis techniques utilizing surface organometallic chemistry (SOMC) techniques to synthesize catalysts that favor high $CH_3OH$ selectivity to increase HC yield.

To summarize, a comprehensive understanding of proximity effects, intermediate transport, active site interactions, and their influence on measured reaction rates and selectivities is paramount for advancing $CO_2$ hydrogenation chemistry. Careful interpretation of these phenomena will continue to be strengthened by increasingly advanced experimental and computational techniques. However, without a strong grasp of these concepts, a lack of comprehension could lead to misleading interpretations. Addressing these fundamental challenges is crucial not only for $CO_2$ hydrogenation chemistry but also for similar sustainable process, such as lignocellulosic biomass conversion, or catalytic upcycling of plastics, both of which contain macromolecules where diffusion constraints and catalyst design remain a critical factor in the production of sustainable fuels and chemicals.

## Concluding remarks

In our perspective, addressing the challenges of $CO_2$ hydrogenation *via* the $CH_3OH$-mediated route requires a paradigm shift in how we interpret catalyst performance—moving beyond activity-selectivity studies to a more mechanistic understanding

of reaction-transport effects and active site interactions. We believe that the site-proximity effects in bifunctional oxide/zeolite systems and the inherent mass transport artifacts of constituent reactions in MTH step should not only be acknowledged but strategically leveraged through rational modification of zeolites to control product selectivity. Additionally, the use of diagnostic selectivity metrics, such as ethylene-to-propylene, ethylene-to-2-methylbutane, and paraffin-to-olefin ratios, *etc.*, can provide deeper insight into hydrocarbon pool (HCP) dynamics, while advanced synthesis strategies like surface organometallic chemistry (SOMC) can help improving $CH_3OH$ yields; together, these approaches can be leveraged to tune hydrocarbon selectivities and yields. As researchers in this field, we see these efforts as essential to bridging current knowledge gaps and guiding the design of next-generation catalytic systems for sustainable $CO_2$ valorization and beyond.

## Data availability

No primary research results, software or code have been included and no new data were generated or analysed as part of this perspective.

## Author contributions

F. M. and M. S. – conceptualization. F. M. – writing-original draft. F. M., A. I. and M. S. – figures, writing, review and editing. M. S – funding acquisition and supervision. All authors contributed to the manuscript.

## Conflicts of interest

There are no conflicts to declare.

## Acknowledgements

## References

1 A. Behr, A. J. Vorholt, K. A. Ostrowski and T. Seidensticker, *Green Chem.*, 2014, **16**, 982–1006.

2 K. T. Dinh, M. M. Sullivan, P. Serna, R. J. Meyer and Y. Roman-Leshkov, *ACS Catal.*, 2021, **11**, 9262–9270.

3 M. Shetty, A. Walton, S. R. Gathmann, M. A. Ardagh, J. Gopeesingh, J. Resasco, T. Birol, Q. Zhang, M. Tsapatsis and D. G. Vlachos, *ACS Catal.*, 2020, **10**, 12666–12695.

4 J. Gopeesingh, M. A. Ardagh, M. Shetty, S. T. Burke, P. J. Dauenhauer and O. A. Abdelrahman, *ACS Catal.*, 2020, **10**, 9932–9942.

5 M. A. Ardagh, M. Shetty, A. Kuznetsov, Q. Zhang, P. Christopher, D. G. Vlachos, O. A. Abdelrahman and P. J. Dauenhauer, *Chem. Sci.*, 2020, **11**, 3501–3510.

6 G. Kumar, E. Nikolla, S. Linic, J. W. Medlin and M. J. Janik, *ACS Catal.*, 2018, **8**, 3202–3208.

7 H. Wu, B. Zhang, H. Liang, L. Zhai, G. Wang and Y. Qin, *Innovation*, 2020, **1**, 100029.

8 E. A. Wilson, S. C. Eady, T. Silbaugh, L. T. Thompson and M. A. Barteau, *J. Catal.*, 2021, **404**, 977–984.

9 J.-C. Wasilke, S. J. Obrey, R. T. Baker and G. C. Bazan, *Chem. Rev.*, 2005, **105**, 1001–1020.

10 M. Muzzio, H. Lin, K. Wei, X. Guo, C. Yu, T. Yom, Z. Xi, Z. Yin and S. Sun, *ACS Sustain. Chem. Eng.*, 2020, **8**, 2814–2821.

11 J. Louie, C. W. Bielawski and R. H. Grubbs, *J. Am. Chem. Soc.*, 2001, **123**, 11312–11313.

12 M. C. Haibach, S. Kundu, M. Brookhart and A. S. Goldman, *Acc. Chem. Res.*, 2012, **45**, 947–958.

13 D. Gorbunov, M. Nenasheva, E. Naranov, A. Maximov, E. Rosenberg and E. Karakhanov, *Appl. Catal., A*, 2021, **623**, 118266.

14 S. D. Drouin, F. Zamanian and D. E. Fogg, *Organometallics*, 2001, **20**, 5495–5497.

15 R. Helmer, S. S. Borkar, A. Li, F. Mahnaz, J. Vito, A. Iftakher, M. F. Hasan, S. Rangarajan and M. Shetty, *Angew. Chem., Int. Ed.*, 2025, **64**, e202416384.

16 R.-P. Ye, J. Ding, W. Gong, M. D. Argyle, Q. Zhong, Y. Wang, C. K. Russell, Z. Xu, A. G. Russell and Q. Li, *Nat. Commun.*, 2019, **10**, 1–15.

17 Y. Wang, G. Wang, L. I. van der Wal, K. Cheng, Q. Zhang, K. P. de Jong and Y. Wang, *Angew. Chem.*, 2021, **133**, 17876–17884.

18 Y. Wang, L. Tan, M. Tan, P. Zhang, Y. Fang, Y. Yoneyama, G. Yang and N. Tsubaki, *ACS Catal.*, 2018, **9**, 895–901.

19 J. Wang, R. Li, G. Zhang, C. Dong, Y. Fan, S. Yang, M. Chen, X. Guo, R. Mu and Y. Ning, *J. Am. Chem. Soc.*, 2024, **146**, 5523–5531.

20 G. Wang, Y. Wang, J. Cao, X. Wang, Y. Yi and F. Liu, *Microporous Mesoporous Mater.*, 2020, **291**, 109693.

21 P. Tian, G. Zhan, J. Tian, K. B. Tan, M. Guo, Y. Han, T. Fu, J. Huang and Q. Li, *Appl. Catal., B*, 2022, **315**, 121572.

22 H. Tian, H. He, J. Jiao, F. Zha, X. Guo, X. Tang and Y. Chang, *Fuel*, 2022, **314**, 123119.

23 D. Tian, Y. Men, S. Liu, J. Wang, Z. Li, K. Qin, T. Shi and W. An, *Colloids Surf., A*, 2022, **653**, 129945.

24 A. Livescu, R. Navar, J. R. Mangalindan, F. Mahnaz, Y. Ge, M. Shetty and X. Yang, *Top. Catal.*, 2024, 1–22.

25 Z. Liu, Y. Ni, T. Sun, W. Zhu and Z. Liu, *J. Energy Chem.*, 2021, **54**, 111–117.

26 P. Gao, S. Li, X. Bu, S. Dang, Z. Liu, H. Wang, L. Zhong, M. Qiu, C. Yang and J. Cai, *Nat. Chem.*, 2017, **9**, 1019–1024.

27 P. Gao, S. Dang, S. Li, X. Bu, Z. Liu, M. Qiu, C. Yang, H. Wang, L. Zhong and Y. Han, *ACS Catal.*, 2018, **8**, 571–578.

28 S. Chen, J. Wang, Z. Feng, Y. Jiang, H. Hu, Y. Qu, S. Tang, Z. Li, J. Liu and J. Wang, *Angew. Chem.*, 2024, **136**, e202316874.

29 J. Chen, X. Wang, D. Wu, J. Zhang, Q. Ma, X. Gao, X. Lai, H. Xia, S. Fan and T.-S. Zhao, *Fuel*, 2019, **239**, 44–52.

30 J. R. Mangalindan, F. Mahnaz, J. Vito, N. Suphavilai and M. Shetty, *ACS Eng. Au*, 2025, e5c00008.

31 F. Mahnaz, J. R. Mangalindan, B. C. Dharmalingam, J. Vito, Y.-T. Lin, M. Akbulut, J. J. Varghese and M. Shetty, *ACS Sustain. Chem. Eng.*, 2024, **12**, 5197–5210.

32 F. Mahnaz, V. Dunlap, R. Helmer, S. S. Borkar, R. Navar, X. Yang and M. Shetty, *ChemCatChem*, 2023, **15**, e202300402.

33 L. Guo, P. Ai, X. Gao, H. Wu, X. Wang, Y. Kugue, J. Liang, W. Gao, X. Guo, J. Sun, *EES Catalysis*, 2023.

34 P. Sharma, J. Sebastian, S. Ghosh, D. Creaser and L. Olsson, *Catal. Sci. Technol.*, 2021, **11**, 1665–1697.

35 K. B. Tan, K. Xu, D. Cai, J. Huang and G. Zhan, *Chem. Eng. J.*, 2023, **463**, 142262.

36 T. Xie, J. Ding, X. Shang, X. Zhang and Q. Zhong, *J. Colloid Interface Sci.*, 2023, **635**, 148–158.

37 Y. Li, L. Zeng, G. Pang, X. Wei, M. Wang, K. Cheng, J. Kang, J. M. Serra, Q. Zhang and Y. Wang, *Appl. Catal., B*, 2023, **324**, 122299.

38 F. Mahnaz, J. R. Mangalindan, J. Vito, R. Helmer and M. Shetty, *J. Catal.*, 2024, **434**, 115518.

39 S. Ilias and A. Bhan, *ACS Catal.*, 2013, **3**, 18–31.

40 S. Ilias and A. Bhan, *J. Catal.*, 2012, **290**, 186–192.

41 A. Hwang and A. Bhan, *Acc. Chem. Res.*, 2019, **52**, 2647–2656.

42 P. B. Weisz, in *Advances in Catalysis*, Elsevier, 1962, vol. 13, pp. 137–190.

43 P. Weisz and E. Swegler, *Science*, 1957, **126**, 31–32.

44 P. Weisz, *Science*, 1956, **123**, 887–888.

45 W. Hu, G. Noh and E. Iglesia, *J. Catal.*, 2023, **425**, 125–142.

46 G. Noh, Z. Shi, S. I. Zones and E. Iglesia, *J. Catal.*, 2018, **368**, 389–410.

47 G. Noh, E. Lam, D. T. Bregante, J. Meyet, P. Šot, D. W. Flaherty and C. Copéret, *Angew. Chem.*, 2021, **133**, 9736–9745.

48 E. Lam, G. Noh, K. W. Chan, K. Larmier, D. Lebedev, K. Searles, P. Wolf, O. V. Safonova and C. Copéret, *Chem. Sci.*, 2020, **11**, 7593–7598.

49 Z. Li, Y. Qu, J. Wang, H. Liu, M. Li, S. Miao and C. Li, *Joule*, 2019, **3**, 570–583.

50 Z. Li, J. Wang, Y. Qu, H. Liu, C. Tang, S. Miao, Z. Feng, H. An and C. Li, *ACS Catal.*, 2017, **7**, 8544–8548.

51 J. C. Gottifredi, E. E. Gonzo and O. Quiroga, *Concept and Design of Chemical Reactors*, 1986.

52 A. Krishna, *Catal. Rev.: Sci. Eng.*, 1990, **32**, 279–381.

53 C. W. Hullfish, J. Z. Tan, H. I. Adawi and M. L. Sarazen, *ACS Catal.*, 2023, **13**, 13140–13150.

54 F. Arena, G. Mezzatesta, G. Zafarana, G. Trunfio, F. Frusteri and L. Spadaro, *J. Catal.*, 2013, **300**, 141–151.

55 H. Hu, J. Zhu, F. Yang, Z. Chen, M. Deng, L. Weng, Y. Ling and Y. Zhou, *Chem. Commun.*, 2019, **55**, 6495–6498.

56 Y. Bhawe, M. Moliner-Marin, J. D. Lunn, Y. Liu, A. Malek and M. Davis, *ACS Catal.*, 2012, **2**, 2490–2495.

57 R. Khare, D. Millar and A. Bhan, *J. Catal.*, 2015, **321**, 23–31.

58 A. Hwang, T. T. Le, Z. Shi, H. Dai, J. D. Rimer and A. Bhan, *J. Catal.*, 2019, **369**, 122–132.

59 Z. Shi and A. Bhan, *J. Catal.*, 2023, **421**, 198–209.

60 M. L. Sarazen, E. Doskocil and E. Iglesia, *ACS Catal.*, 2016, **6**, 7059–7070.

61 Q. Sun, Y.-L. Zhang, H.-Y. Chen, J.-F. Deng, D. Wu and S.-Y. Chen, *J. Catal.*, 1997, **167**, 92–105.

62 S. S. Iyer, T. Renganathan, S. Pushpavanam, M. V. Kumar and N. Kaisare, *J. CO₂ Util.*, 2015, **10**, 95–104.

63 M. Bowker, *ChemCatChem*, 2019, **11**, 4238–4246.

64 I. Nezam, W. Zhou, G. S. Gusmão, M. J. Realff, Y. Wang, A. J. Medford and C. W. Jones, *J. CO₂ Util.*, 2021, **45**, 101405.

65 I. Yarulina, A. D. Chowdhury, F. Meirer, B. M. Weckhuysen and J. Gascon, *Nat. Catal.*, 2018, **1**, 398–411.

66 F. J. Keil, *Microporous Mesoporous Mater.*, 1999, **29**, 49–66.

67 W. Prachumsai, S. Pangtaisong, S. Assabumrungrat, P. Bunruam, C. Nakvachiratrakul, D. Saebea, P. Praserthdam and S. Soisuwan, *J. Environ. Chem. Eng.*, 2021, **9**, 104979.

68 M. Huš, V. D. Dasireddy, N. S. Štefančič and B. Likozar, *Appl. Catal., B*, 2017, **207**, 267–278.

69 Y. Wang, X. Gao, M. Wu and N. Tsubaki, *EcoMat*, 2021, **3**, e12080.

70 D. Zhao, S. Han and E. V. Kondratenko, *ChemCatChem*, 2023, **15**, e202300679.

71 S. Ghosh, J. Sebastian, L. Olsson and D. Creaser, *Chem. Eng. J.*, 2021, **416**, 129120.

72 T. Numpilai, C. Wattanakit, M. Chareonpanich, J. Limtrakul and T. Witoon, *Energy Convers. Manage.*, 2019, **180**, 511–523.

73 A. Beck, M. A. Newton, L. G. van de Water and J. A. van Bokhoven, *Chem. Rev.*, 2024, **124**, 4543–4678.

74 G. Pacchioni, *ACS Catal.*, 2024, **14**, 2730–2745.

75 Y. Yang, C. A. Mims, D. Mei, C. H. Peden and C. T. Campbell, *J. Catal.*, 2013, **298**, 10–17.

76 S. Kattel, B. Yan, Y. Yang, J. G. Chen and P. Liu, *J. Am. Chem. Soc.*, 2016, **138**, 12440–12450.

77 S. Kattel, P. Liu and J. G. Chen, *J. Am. Chem. Soc.*, 2017, **139**, 9739–9754.

78 Z. Shi and A. Bhan, *Chem. Eng. J.*, 2023, **456**, 140867.

79 S. S. Arora, Z. Shi and A. Bhan, *ACS Catal.*, 2019, **9**, 6407–6414.

80 M. Stöcker, *Microporous Mesoporous Mater.*, 1999, **29**, 3–48.

81 R. Singh, K. Tripathi and K. K. Pant, *Fuel*, 2021, **303**, 121289.

82 F. Mahnaz, B. C. Dharmalingam, J. R. Mangalindan, J. Vito, J. J. Varghese and M. Shetty, *Chem. Catal.*, 2025, **5**(2), 101183.

83 H. Chen, H. Cui, Y. Lv, P. Liu, F. Hao and W. Xiong, *Fuel*, 2022, **314**, 123035.

84 G. Ertl, H. Knözinger and J. Weitkamp, *Handbook of heterogeneous catalysis*, VCH Weinheim, 1997, vol. 2.

85 H. G. Karge, *Studies in Surface Science and Catalysis*, 1997, vol. 105, pp. 1901–1948.

86 H. G. Karge, in *Studies in Surface Science and Catalysis*, Elsevier, 1994, vol. 83, pp. 135–146.

87 Y. Wang, F. Liu, M. Yao, J. Ma, S. Geng, J. Cao and X. Wang, *Sep. Purif. Technol.*, 2025, **355**, 129743.

88 H. M. Torres Galvis and K. P. de Jong, *ACS Catal.*, 2013, **3**, 2130–2149.

89 M. G. Sibi, D. Verma and J. Kim, *Catal. Rev.*, 2022, 1–60.

90 G. Ertl, H. Knözinger and J. Weitkamp, *Preparation of solid catalysts*, John Wiley & Sons, 2008.

91 H. G. Karge, H. K. Beyer and G. Borbély, *Catal. Today*, 1988, **3**, 41–52.

92 H. G. Karge, in *Handbook of Heterogeneous Catalysis*, Wiley-VCH, 2008, pp. 484–510.

93 D. Yin and D. Yin, *Microporous Mesoporous Mater.*, 1998, **24**, 123–126.

94 T. Liu, Z. Liu, S. Jiang, P. Peng, Z. Liu, A. D. Chowdhury and G. Liu, *Chem. Soc. Rev.*, 2025, **54**, 2726–2761.

95 Y. Yue, J. Tian, J. Ma, S. Yang, W. Li, J. Huang, Q. Li and G. Zhan, *Appl. Catal., B*, 2024, **355**, 124158.

96 Y. Ono, H. Adachi and Y. Senoda, *J. Chem. Soc., Faraday Trans. 1*, 1988, **84**, 1091–1099.

97 D. Esquivel, A. J. Cruz-Cabeza, C. Jimenez-Sanchidrian and F. J. Romero-Salguero, *Microporous Mesoporous Mater.*, 2013, **179**, 30–39.

98 E. A. Redekop, T. Cordero-Lanzac, D. Salusso, A. Pokle, S. Oien-Odegaard, M. F. Sunding, S. Diplas, C. Negri, E. Borfecchia and S. Bordiga, *Chem. Mater.*, 2023, **35**, 10434–10445.

99 Y. Yuan, E. Huang, S. Hwang, P. Liu and J. G. Chen, *Nat. Commun.*, 2024, **15**, 6529.

100 S. Xing, S. Turner, D. Fu, S. van Vreeswijk, Y. Liu, J. Xiao, R. Oord, J. Sann and B. M. Weckhuysen, *JACS Au*, 2023, **3**, 1029–1038.

101 X. Ren, S. Yang, R. Xu, M. Guo, W. Huang, M. Ding and J. Zhong, *J. Membr. Sci.*, 2022, **643**, 119998.

102 R. P. Townsend, E. N. Coker, in *Studies in surface science and catalysis*, Elsevier, 2001, vol. 137, pp. 467–524.

103 A. V. Kucherov and A. A. Slinkin, *J. Mol. Catal.*, 1994, **90**, 323–354.